Science of the Total Environment 782 (2021) 146571

Contents lists available at ScienceDirect

Science of the Total Environment

journal homepage: www.elsevier.com/locate/scitotenv

Characterization of the vehicle emissions in the Greater Taipei Area through vision-based traffic analysis system and its impacts on urban air quality

I-Chun Tsai [a,*], Chen-Ying Lee [a], Shih-Chun Candice Lung [a], Chih-Wen Su [b]

[a] Research Center for Environmental Changes, Academia Sinica, Taipei, Taiwan, ROC
[b] Department of Information and Computer Engineering, Chung Yuan Christian University, Taoyuan City, Taipei, Taiwan, ROC

HIGHLIGHTS

- Vehicle emissions for the Greater Taipei Area obtained from a vision-based traffic analysis system
- Sedans were the most common vehicles in the Greater Taipei Area, followed by motorcycles.
- The addition of real-time traffic data improved the model performance.
- Vehicle emissions contributed to >90% CO, 80% NOx, and 50% $PM_{2.5}$.
- Vehicle emissions contribution in the Greater Taipei Area affected by both emission and meteorology

GRAPHICAL ABSTRACT

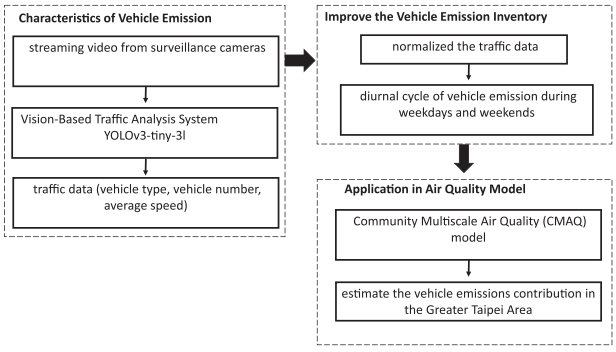

ARTICLE INFO

Article history:
Received 17 January 2021
Received in revised form 1 March 2021
Accepted 15 March 2021
Available online 23 March 2021

Editor: Pavlos Kassomenos

Keywords:
Vehicle emissions
Urban air quality
Vision-based traffic analysis system
You Only Look Once
Community Multiscale Air Quality (CMAQ) model

ABSTRACT

In recent years, many surveillance cameras have been installed in the Greater Taipei Area, Taiwan; traffic data obtained from these surveillance cameras could be useful for the development of roadway-based emissions inventories. In this study, web-based traffic information covering the Greater Taipei Area was obtained using a vision-based traffic analysis system. Web-based traffic data were normalized and applied to the Community Multiscale Air Quality (CMAQ) model to study the impact of vehicle emissions on air quality in the Greater Taipei Area.

According to an analysis of the obtained traffic data, sedans were the most common vehicles in the Greater Taipei Area, followed by motorcycles. Moderate traffic conditions with an average speed of 30–50 km/h were most prominent during weekdays, whereas traffic flow with an average speed of 50–70 km/h was most common during weekends. The proportion of traffic flows in free-flow conditions (>70 km/h) was higher on weekends than on weekdays. Two peaks of traffic flow were observed during the morning and afternoon peak hours on weekdays. On the weekends, this morning peak was not observed, and the variation in vehicle numbers was lower than on weekdays.

The simulation results suggested that the addition of real-time traffic data improved the CMAQ model's performance, especially for the carbon monoxide (CO) and fine particulate matter ($PM_{2.5}$) concentrations. According to sensitivity tests for total and vehicle emissions in the Greater Taipei Area, vehicle emissions contributed to >90% of CO, 80% of nitrogen oxides (NO_x), and approximately 50% of $PM_{2.5}$ in the downtown areas of Taipei. The vehicle emissions contribution was affected by both vehicle emissions and meteorological conditions. The connection between the surveillance camera data, vehicle emissions, and regional air quality models in this study can also be used to explore the impact of special events (e.g., long weekends and COVID-19 lockdowns) on air quality.

* Corresponding author at: Research Center for Environmental Changes, Academia Sinica, 128 Academia Road, Section 2, Nankang, Taipei 11529, Taiwan, ROC.
E-mail address: ictsai@gate.sinica.edu.tw (I.-C. Tsai).

https://doi.org/10.1016/j.scitotenv.2021.146571

1. Introduction

The emissions of nitrogen oxides (NOx), carbon monoxide (CO), and volatile organic compounds from vehicles are recognized as the main precursors of ozone and secondary organic aerosols in metropolitan areas (Nagpure et al., 2013). Urban-scale fine particulate matter ($PM_{2.5}$) from vehicle emissions are also receiving increasing attention in assessments of emissions and the associated health risks. According to a report published by the European Environment Agency, road transport contributes up to 30% of particulates in European Union cities, up to 40% of NOx, and up to 19% of CO (EEA, 2019). With the urbanization of Taiwan in the 1970s, vehicle emissions have become a critical source of air pollution in metropolitan areas (Anenberg et al., 2017; Liu et al., 2017). Therefore, an accurate estimate of vehicle emissions is essential for air quality modeling and policymaking.

Many emissions inventories with different temporal and spatial scales (e.g., global, regional, and urban) have been developed, such as MOtor Vehicle Emission Simulator (EPA, 2010), EMFAC2017 (California Air Resources Board, 2018), the International Vehicle Emissions model (Davis et al., 2005)), and the Taiwan Emission Data System (https://teds.epa.gov.tw). Conventional vehicle emission inventories are based on laboratory like bench tests, remote sensing, or tunnel experiments (Ning and Chan, 2007; Silva et al., 2016; Zhang et al., 2015). The tunnel approach is the most widely used method for studying pollutant emissions from urban vehicle exhausts in the real world. Because experiments conducted in tunnels are generally unaffected by the external environment, the results can reflect the pollutant emission characteristics of different vehicles under different driving conditions (Cui and Nelson, 2019; Deng et al., 2018; Marinello et al., 2020). The temporal and spatial scales of urban vehicle emissions vary widely. However, tunnel experiments can only estimate the emission of a few types of vehicles at a time, and they are very expensive (Marinello et al., 2020). Therefore, considerable uncertainty remains regarding inter- and intra- vehicle emissions due to differences in vehicle type, vehicle speed, driving cycle, roadway condition, and other parameters.

In recent years, real-time traffic data, such as floating car data, mobile monitoring data, and online ridesourcing service data, have been used to collect traffic information and improve roadway-based emissions inventories (Jing et al., 2016; Li et al., 2019; Sun and Ding, 2019). Meng et al. (2020) evaluated web-based real-time traffic data by using real-world measurements. They suggested using web-based traffic data in transportation and environmental research. Jing et al. (2016) combined a road transport model with near-real-time traffic data to develop a vehicle emissions inventory with high temporal and spatial resolution for the Beijing urban area.

In Taiwan, many surveillance cameras have been installed in various cities. In this study, web-based real-time images from surveillance cameras in the Greater Taipei Area, Taiwan, were collected and analyzed using a vision-based traffic analysis system. In this analysis system, a one-stage object detection method was used to quickly detect and track vehicles and thus obtain accurate traffic data (Wang et al., 2020a, 2020b). Then, traffic data characteristics during weekdays and weekends were used to improve urban emission inventories and an air quality model. More details about the traffic analysis system and a description of the air quality model can be found in Section 2. Section 3 presents an analysis of the traffic data and the simulation results related to vehicle emission contributions.

The variation in vehicle emissions in urban areas was significant, and the high spatiotemporal resolution of real-time traffic data enabled the presentation of local human and vehicle activities. The demonstrated connection between surveillance camera data, vehicle emissions, and regional air quality models can improve the emission inventories and elucidate the impacts of special events on air quality. For example, coronavirus disease 2019 (COVID-19) was first reported in late December 2019 in China. In the following months, the virus spread rapidly in other parts of the world due to the movement of people traveling by aircraft or high-speed train. Marinello et al. (2021) measured the number of vehicles in Reggio Emilia, Italy, and found a rapid decline in vehicle numbers during 2020 by up to 82%. It led to a > 30% reduction in NO_2 and a 22% reduction in CO in the air. Filonchyk et al. (2020) and Wang et al. (2021) have analyzed satellite data and in-situ observations of NO_2 and CO over East China during 2019 and 2020. They have observed significant declines in NO_2 and CO due to the COVID-19 lockdown. The method proposed in the present study can be used quickly to improve vehicle emission inventories and accurately estimate air quality.

2. Methodology

Fig. 1 presents flowchart of the methods used in this study. Web-based traffic information for the Greater Taipei Area was obtained using a vision-based traffic analysis system. The web-based traffic data were normalized, and the normalized diurnal cycle of vehicle emissions was applied to the Community Multiscale Air Quality (CMAQ) model to investigate the impact of vehicle emissions on air quality in the Greater Taipei Area.

2.1. Web-based real-time traffic data

Real-time traffic data were acquired from the Taipei City Advanced Traveler Information System Web (http://its.taipei.gov.tw). Real-time

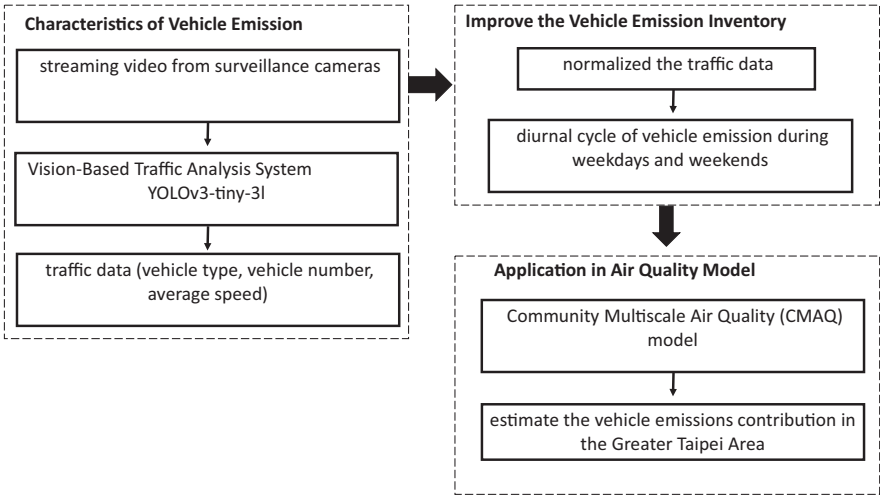

Fig. 1. Flowchart of the methods used in this study, including the vision-based traffic analysis system and the air quality model.

images from surveillance cameras were then processed through a modified lightweight convolutional neural network (CNN)-based architecture—version 3 of You Only Look Once (YOLOv3-tiny-3 l, Alexey/AB, 2020) to acquire real-time traffic data. Current object detection methods based on deep learning can be categorized based on whether two- or one-stage object detectors are used. Although the accuracy of two-stage detectors is usually higher than that of one-stage detectors, the detection speed is limited at the classification stage. YOLOv3-tiny-3 l is a modified lightweight version of YOLOv3 (Redmon and Farhadi, 2018), a state-of-the-art one-stage object detection method. The detection accuracy of YOLOv3 is sufficiently high, but the inference time and model size are unsuitable for analyzing multiple streaming videos in practice. YOLOv3-tiny-3 l reduces the number of layers to seven convolutional layers and six pooling layers, but it preserves the feature pyramid network structure. This simplified network can be used to perform efficient object detection without a substantial reduction in accuracy compared with YOLOv3 (Alexey/AB, 2020; Wang et al., 2020a; Wang et al., 2020b). Wang et al. (2020b) tested YOLOv3-tiny-3 l on KITTI data sets, and the average accuracy was 88%. The detection speed of YOLOv3-tiny-3 l is 170 frames/s, and it meets real-time application requirements.

After YOLOv3-tiny-3 l predicted the position and type of each vehicle, the optical flow technique was used to track the feature points inside the vehicle area. Sufficient representative training data are crucial for a reliable and robust deep learning model, and these data must be manually labeled. Therefore, traffic images containing vehicles with as wide a variety of appearances as possible should be first obtained from surveillance cameras. In this study, the vehicles were assigned to five categories: sedan, motorcycle, bus, truck, and trailer. The resolution and quality of videos recorded by surveillance cameras in Taiwan is usually low (352 × 240 px); before feather extraction using the CNN, the images were resized to 608 × 608 px. In the training phase, 2439 images from 23 surveillance cameras in Greater Taipei Area were used to train the model. As reported by Wang et al. (2020a, 2020b), YOLOv3-tiny-3 l has precision and recall rates of 87% and 84%, respectively, for five vehicle types. For sedans, the most common vehicles in Greater Taipei Area, the precision and recall rates were both higher than 89%.

The locations of surveillance cameras showing heavy traffic are shown in Fig. 2a. Raw images of web-based real-time traffic data were obtained during March, June, August, September, and October of 2019. After processing the images using YOLOv3-tiny-3 l, we obtained a time series of traffic data variations which are discussed in Section 3.1.

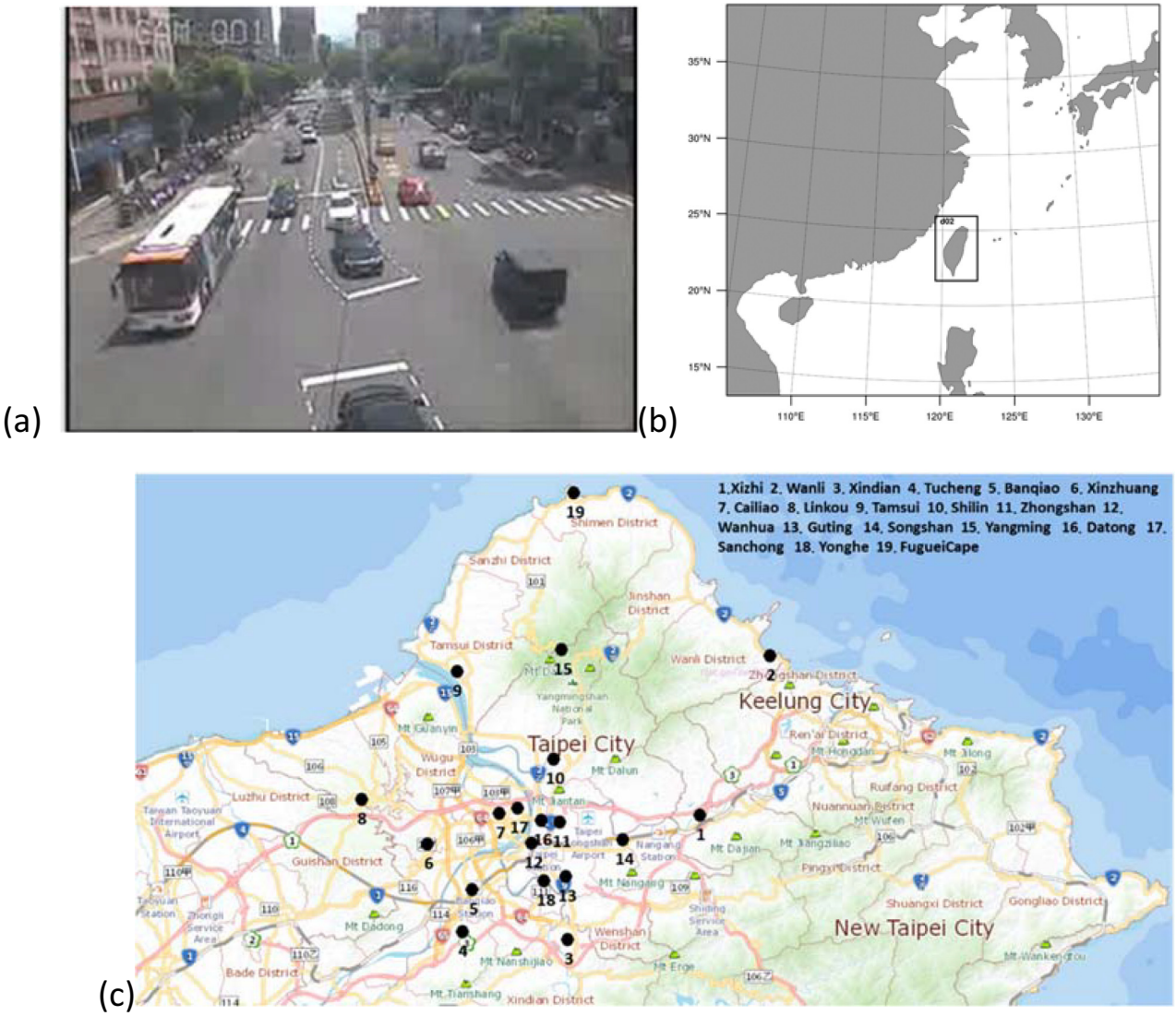

Fig. 2. (a) Real-time surveillance camera images that were processed using YOLOv3-tiny-3 l. (b)Geographic distribution of simulated domains. The resolution of the outer domain was 10 km, and it covered the region from 100°E to 140°E and 15°E to 40°N. The resolution of the inner domain was 2 km. (c) Locations of TWEPA stations (1 to 19) and main roads in the Greater Taipei Area.

Table 1
Three scenarios for the diurnal cycles of vehicle emissions used in the simulations.

EXP	
WEEKDAY	The diurnal cycle of vehicle emissions was the same during the weekdays and weekends.
WEEKEND	The diurnal cycle of vehicle emissions during weekends was obtained from the vision-based traffic analysis system.
WEEKEND_tra	Same as WEEKEND, but only vehicle emissions were considered.

2.2. Vehicle emission scenarios and air quality model

The Community Multiscale Air Quality (CMAQ) model, version 4.7.1 (Byun and Schere, 2006), developed by the United States Environmental Protection Agency, was adopted to simulate the impacts of vehicle emissions on urban-scale air quality. The CMAQ model is a three-dimensional Eulerian model that includes emissions, chemistry, wet and dry deposition, and transport of trace gases and aerosol particles. Meteorological parameters were obtained from simulation results of the National Center for Atmospheric Research Weather Research and Forecasting (WRF) model, version 3.7.1 (Skamarock et al., 2008). In this study, simulations were conducted for the period of March 1–30, 2019. Two domains were used in these simulations, as shown in Fig. 2b. The resolution of the outer domain was 10 km, covering the region from 100°E to 140°E and 15°N to 40°N. The inner domain had a resolution of 2 km and covered Taiwan. The vertical resolution followed a sigma coordinate with 37 layers from surface to 50 Pa. The initial and boundary conditions for the WRF simulation were adopted from the fifth generation of European reanalysis data (ERA5) produced by the European Centre for Medium-Range Weather Forecasts (Hersbach and Dee, 2016). Wind, temperature, and water vapor in the ERA5 data were assigned into coarse domains every 6 h. Physical parameterizations adopted in this study included the Goddard GCE microphysical scheme (Tao et al., 2003), RRTMG shortwave and longwave radiation parameterization (Iacono et al., 2008), the unified Noah land-surface model (Tewari et al., 2004), and the Yonsei University planetary boundary layer scheme (Hong et al., 2006).

For the CMAQ model, the gas-phase chemistry mechanism used in this study was SAPRC-99 (Carter, 2000). Photolysis rates were estimated based on the simulated clear-sky photolysis ratio and then corrected for cloud cover. The formation of secondary organic aerosols through the irreversible uptake of dicarbonyls (glyoxal and methylglyoxal) by wet aerosols and cloud droplets was also considered in the CMAQ model (Fu et al., 2008). This formation pathway may be important in the Pearl River Delta region (Li et al., 2013) and Taiwan (Tsai et al., 2015).

Anthropogenic emissions for China and East and South Asia were acquired from the inventories developed by Li et al. (2017) and Wiedinmyer et al. (2011), respectively. For Taiwan, the emissions were obtained from the 1-km-resolution anthropogenic emission inventory of the Taiwan Emission Data System, version 8.1 (https://teds.epa.gov.tw/), which is supported by the Taiwan Environmental Protection Administration (TWEPA). Point, line, and area sources are included in this database, with a spatial resolution of 1 km for line and area sources and 1 m for point sources. Vehicle emissions in TEDS8.1 are line sources classified into 10 sectors, including heavy-duty diesel trucks, passenger cars, two-stroke motorcycles, and four-stroke motorcycles. The emissions inventory for line sources was estimated using the emission factor method, with the emission factors of pollutants calculated using the MOBILE model version 6.2 (EPA, 2010). Biogenic emissions in the model domain were calculated using the Model of Emissions of Gases and Aerosols from Nature (Guenther et al., 2006), which is driven by meteorological data from WRF simulations and land cover data from NASA MODIS data.

Vehicle numbers vary substantially in metropolitan areas, but the diurnal cycles of vehicle emissions are not provided in TEDS8.1. In this study, we used three scenarios for the diurnal cycles of vehicle emissions to estimate the impacts of vehicle emissions on air quality in the Greater Taipei Area (Table 1). In the WEEKDAY run, the diurnal cycles for weekdays and weekends were the same. By contrast, in the WEEKEND run, the diurnal cycles for weekends were obtained from the web-based real-time traffic data. To explore the role of vehicle emissions on air quality in the Greater Taipei Area, the WEEKEND_tra run included only vehicle emissions.

In this study, observations of meteorological parameters were used to verify the performance of the WRF model. Observations for the Greater Taipei Area during March 2019 were obtained from Taiwan's Central Weather Bureau (CWB; https://www.cwb.gov.tw/eng/index.htm). Hourly meteorology parameters included 2-m temperature (T2), 2-m relative humidity (RH2), sea level pressure (SLP), 10-m wind speed (WS), and wind direction (WD). The hourly concentrations of $PM_{2.5}$, CO, and NO_x obtained from TWEPA stations around the Greater Taipei area were used to evaluate the air quality data simulated by the CMAQ model, as shown in Fig. 2c. Information on TWEPA stations, including land use, sample height (m), and distance to the main road (m), are listed in Table 2.

3. Results and discussions

3.1. Traffic characteristics in the Greater Taipei Area

The mean traffic flow and fleet vehicle compositions derived from the vision-based traffic analysis system in Greater Taipei Area in March 2019 are shown in Fig. 3. The most common vehicles were sedans (>70%), followed by motorcycles (approximately 15%). The vehicle compositions differed between weekdays and weekends. The percentage of sedans in stopped-flow (<10 km/h) and free-flow conditions was lower on weekends than on weekdays.

Table 2
Characteristics of TWEPA stations.

	Land use	Sampling height (m)	Shortest distance to main road (m)		Land use	Sampling height (m)	Shortest distance to main road (m)
Xizhi	Urban	13.5	20	Zhongshan	Urban	20.5	25
Wanli	Permanent wetland	31.5	20	Wanhua	Urban	19.5	30
Xindian	Urban	17.5	0	Guting	Urban	19.5	0
Tucheng	Urban	17.5	50	Songshan	Urban	19.5	20
Banqiao	Urban	19.5	30	Yangming	Evergreen Broadleaf Forest	4.5	10
Xinzhuang	Urban	17.5	50	Datong	Urban	6.5	5
Cailiao	Urban	17.5	20	Sanchong	Urban	3.5	0
Linkou	Urban	19.5	100	Yonghe	Urban	3.5	7
Tamsui	Urban	4.5	0	FugueiCape	Water	0	0
Shilin	Urban	21.5	35				

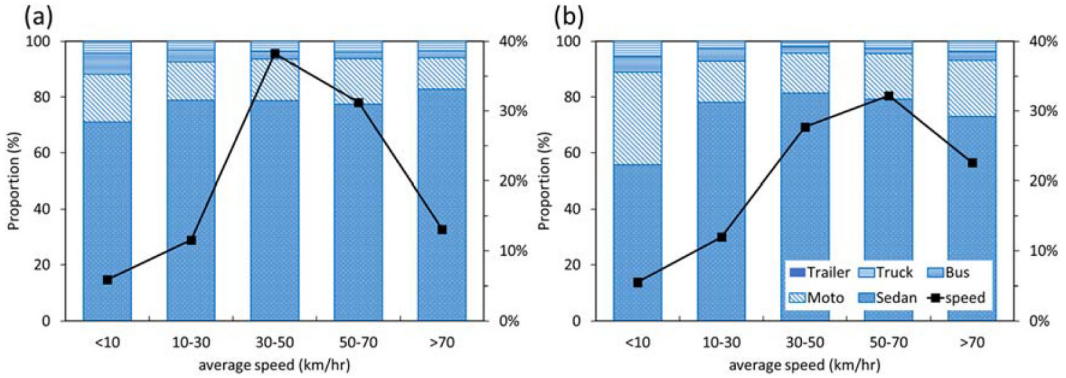

Fig. 3. The proportion of mean speed (black line, km/h) and vehicle compositions (vertical bars, %) from vision-based traffic analysis during (a) weekdays and (b) weekends.

The average speed was approximately 30–70 km/h. The proportion of traffic flow in slow-flow conditions (<30 km/h) was similar on weekdays and weekends. Moderate traffic (30–50 km/h) was the most common traffic flow during weekdays (38% of total vehicles, Fig. 3a), whereas traffic flow with an average speed of 50–70 km/h predominated during weekends (32% of total vehicles, Fig. 3b). The proportion of free-flow traffic conditions (>70 km/h) was higher on weekends than on weekdays. Traffic flow was determined based on the average speed and number of vehicles. In moderate traffic conditions (30–70 km/h), the number of vehicles is relatively high, and vehicles maintain their speed. It resulted in high traffic flow in the moderate traffic condition. In free-flow and slow-flow conditions, the traffic flow was low due to low traffic demand or long idling time.

The mean diurnal cycle of traffic flows and average speed during March 2019 are shown in Fig. 4a. Two peak traffic periods were identified in the Greater Taipei Area on weekdays: in the morning between 7:00 and 9:00 a.m. and the afternoon starting from 5:00 p.m. During off-peak hours, especially between midnight and 5:00 a.m., the number of vehicles was considerably lower (fewer than 60 vehicles during a 5-min period) than during peak hours (more than 100 vehicles during a 5-min period). The average speed was inversely proportional to the number of vehicles. The average speed of >50 km/h in the early morning and decreased rapidly as the number of vehicles increased after 7:00 am. The diurnal cycle of hourly vehicle numbers differed significantly between weekdays and weekends. Two peaks were observed for weekdays during the morning and afternoon. By contrast, no morning peak of vehicle numbers was observed on weekends, and the peak of vehicle numbers in the afternoon on weekends was more than that on weekdays.

3.2. Normalized temporal variations in vehicle emissions

To apply the web-based real-time traffic data to the CMAQ model, we normalized the diurnal cycles of vehicle numbers (Fig. 4a) by using the following formula:

$$R_{t,i} = 24 \cdot \frac{\overline{N_{vt,i}}}{\sum_{t=0}^{23} \overline{N_{vt,i}}} \quad (1)$$

where $R_{t,i}$ is the emission fraction for vehicle type i for 1 day, and $\overline{N_{vt,i}}$ is the mean number of vehicles of vehicle type i at time t in March 2019.

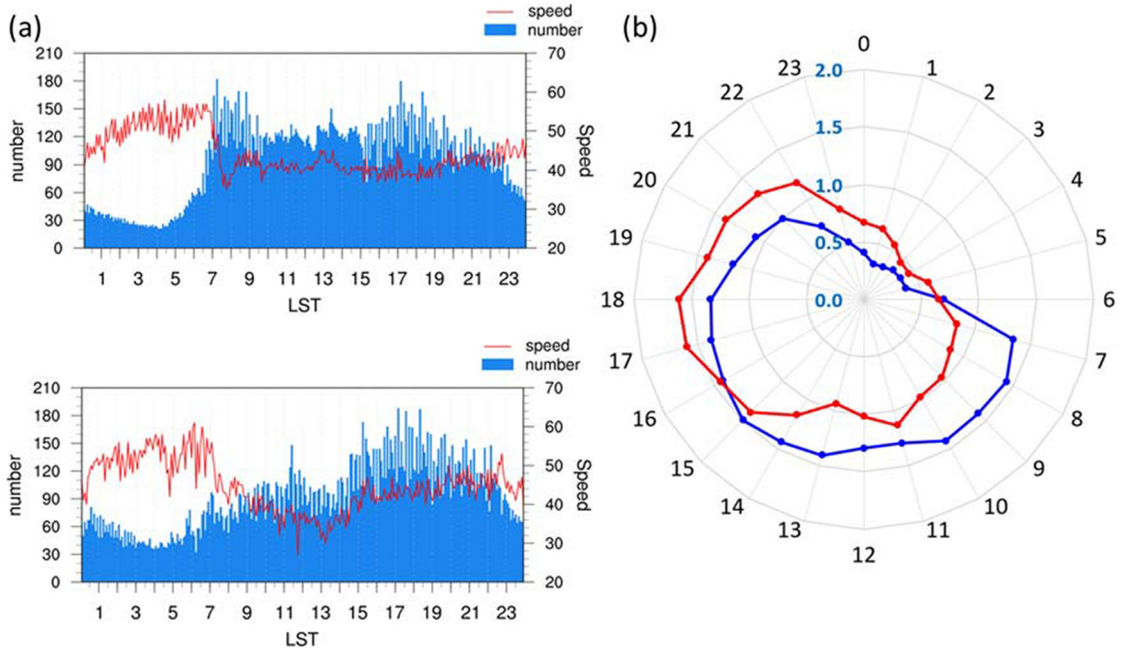

Fig. 4. (a) Mean diurnal cycles of total vehicle numbers (blue bar, number of vehicles during a 5-min period) and average speed (red line, km/h) of traffic flows on weekdays (upper panel) and weekends (lower panel) during March 2019. (b) Normalized diurnal cycles of the number of vehicles during weekdays (blue line) and weekends (red line). (For interpretation of the references to color in this figure legend, the reader is referred to the web version of this article.)

The normalized diurnal cycles of the number of vehicles in this study are shown in Fig. 4b. The difference between the diurnal cycles during weekdays and weekends reveals changes in human activity. For example, the proportion of vehicles number in the morning was higher during weekdays than during weekends. By contrast, the fraction of the number of vehicles after 5:00 p.m. was higher during weekends than during weekdays. This is because people sleep in and stay out later during weekends. These results suggest that real-time traffic data have a high spatiotemporal resolution and can represent local-scale human and vehicle activity. Parameterizing the real-time traffic data into an urban-scale emissions inventory would improve the accuracy of air quality modeling.

3.3. Model evaluation

The normalized diurnal cycles of vehicle emissions shown in Fig. 4b were applied to the CMAQ model, and the role of vehicle emissions in urban air quality is discussed. The quality of a meteorological simulation is essential for the accuracy of air quality data. March 2019 was marked by typical spring weather, with rapid changes in the weather system. Several fronts and continental air masses passed over Taiwan during this month (yellow shading in Fig. 5e), and the prevailing wind was easterly or northeasterly (360°-100°). Under the influence of fronts and moisture from southern China, significant rainfall occurred during 7–10 and 23–25 March. Comparisons of hourly simulated and measured SLP, T2, RH2, WS, and WD at Taipei station from the CWB (Fig. 5) indicated that the WRF model reproduced the observed meteorological parameters with reasonable accuracy. The correlation coefficient (R) of SLP and T2 was >0.9, and that of WS and WD was approximately 0.7–0.8 during this period.

The $PM_{2.5}$, CO, and NO_x are major concerns because vehicle emissions contribute to more than half of their total emissions in the Greater Taipei Area. Fig. 6 presents a time series of the simulated and observed hourly $PM_{2.5}$, CO, and NO_x concentrations at stations in the Great Taipei Area during March 2019. For weekdays (blue line) and weekends (red line), the CMAQ model overestimated the $PM_{2.5}$ concentration and slightly underestimated the CO and NO_x concentrations. In the WEEKEND run, the diurnal fraction of vehicle emissions were obtained from the vision-based traffic analysis system. The correlation coefficients between the simulated and observed daily mean concentrations

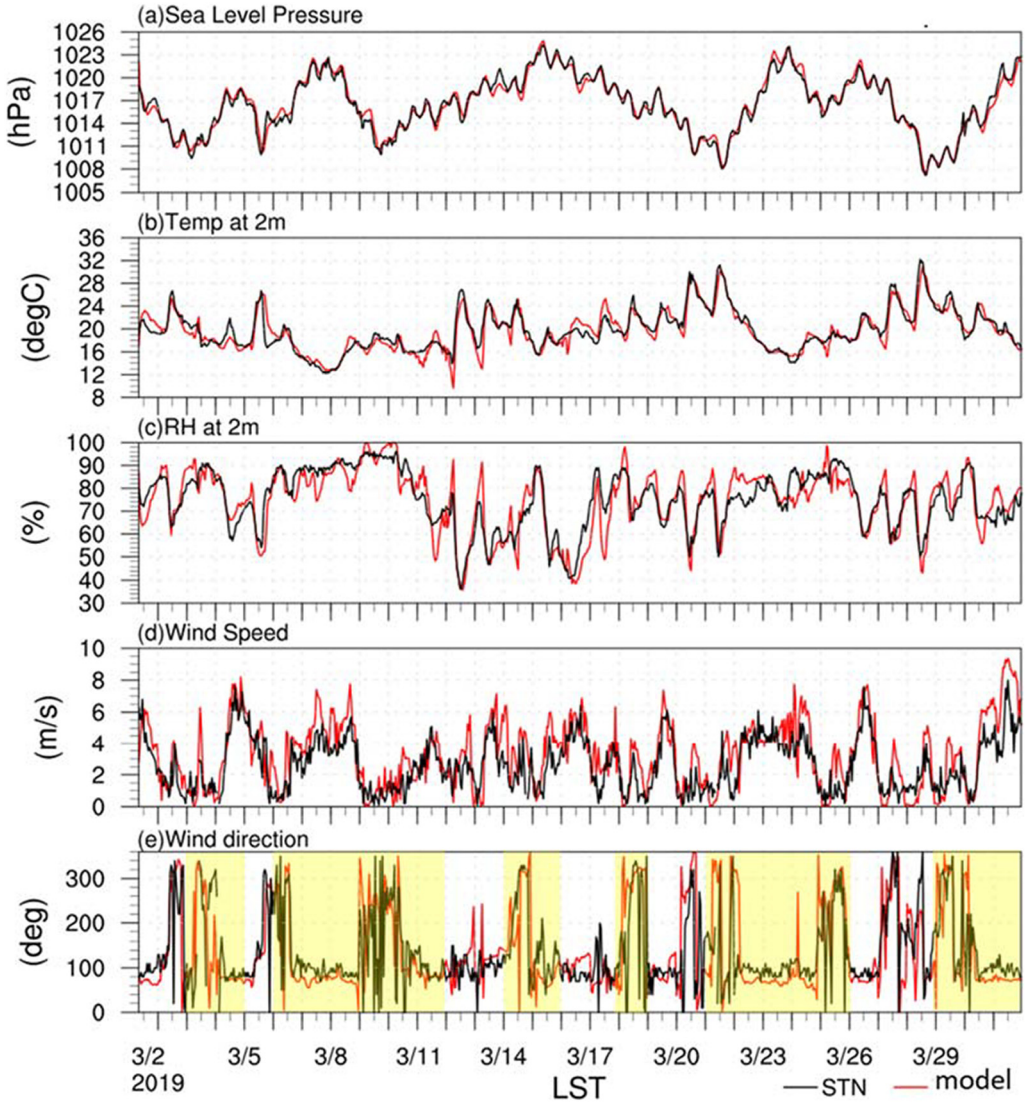

Fig. 5. Comparisons of hourly simulated and measured results of (a) sea level pressure (SLP, hPa), (b) 2-m temperature (T2, K), (c) 2-m relative humidity (RH2, %), (d) 10-m wind speed (WS, m/s), and (e) wind direction (WD, °) for Taipei station from the CWB during March 2019. The yellow shading represents the period during which the weather was influenced by fronts or continental air masses. (For interpretation of the references to color in this figure legend, the reader is referred to the web version of this article.)

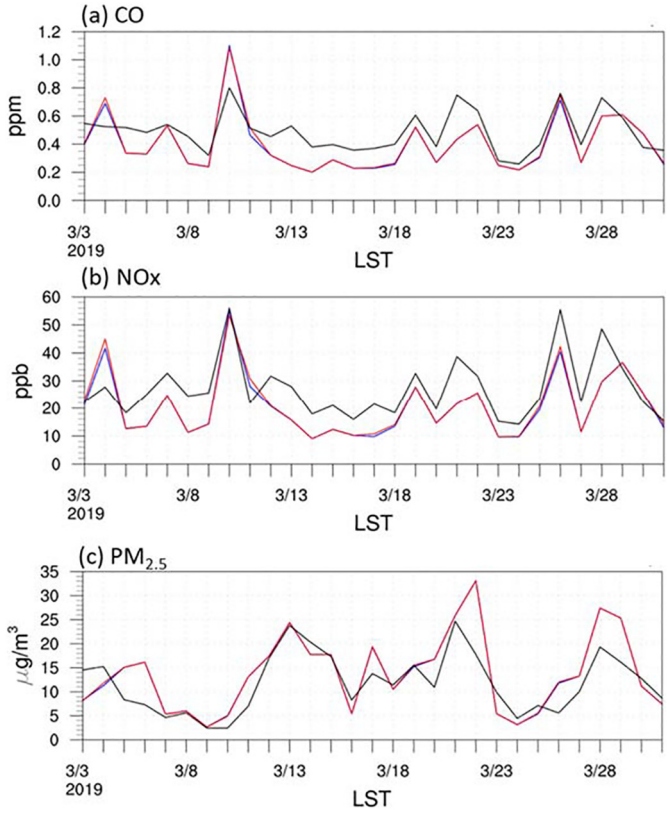

Fig. 6. Time series of simulated (red line denotes the weekend run and blue line denotes the weekday run) and observed (black line) results for the daily mean concentrations of (a) CO (ppm), (b) NOx (ppb), and (c) $PM_{2.5}$ (μg/m^3) at stations in the Taipei metropolitan area during March 2019. (For interpretation of the references to color in this figure legend, the reader is referred to the web version of this article.)

of $PM_{2.5}$, CO, and NO_x at all stations during March 2019 were approximately 0.50, 0.67, and 0.63, respectively; the CMAQ model was consistent with the observations.

3.4. Impact of the diurnal cycle of emissions on weekends

CO forms when the carbon in fuel is only partially oxidized. In the Greater Taipei Area, up to 95% of CO emissions may come from vehicle exhaust. This is a suitable indicator to estimate the impact of the diurnal cycle of emissions during weekends because its lifetime is longer than those of NO_x and $PM_{2.5}$. Fig. 7 presents changes in the correlation coefficients between observed and simulated concentrations of CO, NO_x, and $PM_{2.5}$ due to the diurnal cycle of weekend emissions. For CO, the correlation increased by more than 5% at Xindian, Guting, and Songshan stations, but it decreased by approximately 5% at Cailiao and Sanchong stations. In March 2019, the prevailing wind was easterly or northeasterly (Fig. 5). Xindian, Guting, and Songshan stations are located upstream of the Taipei Basin, and the concentration was dominated by emissions rather than advection. The increased *R* value for CO suggested that the real-time traffic data improved the CMAQ model's performance.

NO_x is a mixture of NO and NO_2; approximately 75% of NO_x emissions are due to vehicle exhaust in the Greater Taipei Area. Although vehicle emissions are a major source of NO_x in urban areas, the results for NO_x were less satisfactory than those of CO and $PM_{2.5}$ were for the diurnal cycle of emissions during weekends. A similar situation was reported by He et al. (2016). This might be due to the prominent local characteristics and short lifetime of ambient NO_x. The lifetime of NO_x is short, and the sub-grid characteristics of NO_x emissions could not be represented. Approximately 40% of $PM_{2.5}$ emissions are due to vehicle emissions in the Greater Taipei Area. $PM_{2.5}$ concentration is determined by complex chemical reactions. The $PM_{2.5}$ concentration results at all stations indicated that the estimated diurnal cycle of $PM_{2.5}$ was slightly improved in the WEEKEND run, with an increase of approximately 3% in the temporal correlation.

Overall, the WEEKEND run had better performance for the Greater Taipei Area, and it was used as the baseline in the subsequent analyses. Notably, the uncertainties in other sectors, such as industrial and residential emissions and emissions in surrounding areas, could still bias the simulated concentrations.

3.5. Effect of vehicle emissions on air quality in the Greater Taipei Area

The contribution of vehicle emissions to ambient pollutant concentrations in the Greater Taipei Area, R_{tra}, was obtained from the simulation results of WEEKEND_tra and the WEEKEND run as follows:

$$R_{tra} = \frac{C_{WEEKEND\_tra}}{C_{WEEKEND}} \times 100\% \quad (2)$$

where C represents the concentration of pollutants. A R_{tra} value close to 100% suggests that the pollutants were mainly attributable to vehicle emissions.

Fig. 8a and b present the spatial distribution of the mean pollutant concentrations based on the WEEKEND and WEEKEND_tra runs. The pollutants were concentrated in downtown Taipei (rectangles in Fig. 8a). The CO and NOx concentrations based on the WEEKEND_tra

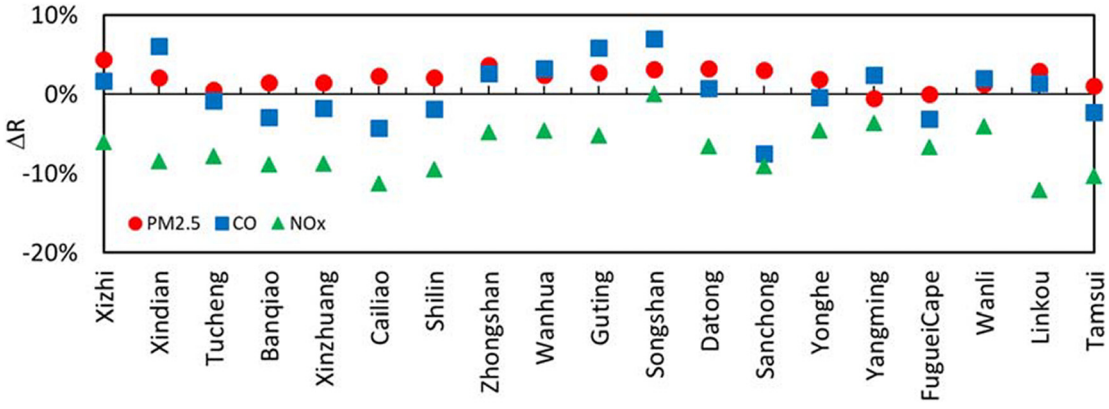

Fig. 7. Changes in the correlation coefficients for $PM_{2.5}$ (red circle), CO (blue square), and NOx (green triangle) concentrations due to the diurnal cycle of weekend emissions (the WEEKEND run minus the WEEKDAY run) during March 2019. (For interpretation of the references to color in this figure legend, the reader is referred to the web version of this article.)

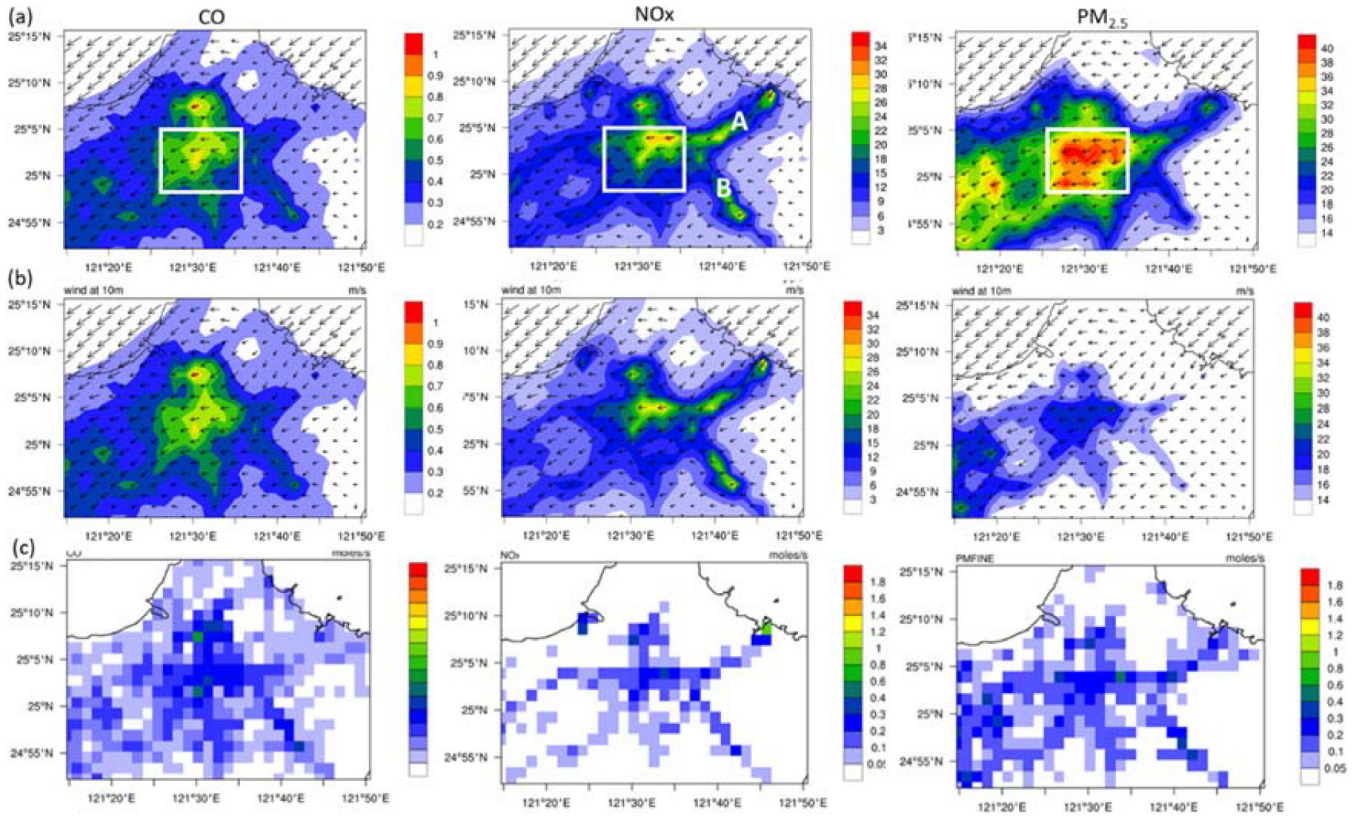

Fig. 8. Spatial distribution of the simulated mean concentration based on (a) the WEEKEND run and (b) the WEEKEND_tra run in Great Taipei Area in March 2019; left to right: CO (ppm), NOx (ppb), and $PM_{2.5}$ (μg/m^3). (c) Emission rate (moles/s). Arrows represent the 10-m wind speed and direction.

run (Fig. 8b) were similar to the WEEKEND run results (Fig. 8a). During March 2019, vehicle emissions contributed >95% of CO and 80% of NO_x in downtown areas. The contribution of vehicle emissions to $PM_{2.5}$ (approximately 50%) was considerable lower than the contributions to CO and NO_x because of the diversity of $PM_{2.5}$ sources. There were several highways around the Greater Taipei area (points A and B in Fig. 8a), and high R_{tra} values of 99% for CO, 95% for NO_x, and 90% for $PM_{2.5}$ were simulated near these highways.

The time series of R_{tra} (Fig. 9) in EPA stations reveals that the contribution of vehicle emissions to pollutants was significantly affected by meteorological conditions. The mean R_{tra} for CO in EPA stations was 99% during March 2019 (Fig. 9a). The mean R_{tra} for NO_x was 87%, with a range of 80%–95% (Fig. 9b). For $PM_{2.5}$, R_{tra} ranged from 35% to 85%, with a mean contribution of 58%. The R_{tra} values for CO remained steady except for two declines during March 20–21 and 27–28. It was mainly due to the southeasterly and southerly winds during these two periods (Fig. 5e), and vehicle emissions were weak outside downtown areas (Fig. 8c). The variation in R_{tra} for NO_x was more significant than that for CO, and the relationship between the R_{tra} for NO_x and wind direction was weaker than that between the R_{tra} for CO and wind direction. This is because of the short lift time of NOx and because the R_{tra} for NOx was affected by local emission sources more than the R_{tra} for CO was. The variation in R_{tra} for $PM_{2.5}$ (Fig. 9c) was greater than those for the other two pollutants. The emission sources for $PM_{2.5}$ were diverse, and R_{tra} was affected not only by wind but also by other meteorological conditions (e.g., precipitation during March 7–10) and other emission sources. Notably, the mixing layer height influences the concentration of pollutants, and their correlation was approximately −0.5 during March 2019. It is because pollutants are trapped near the surface when the mixing layer height was low. However, the correlation between R_{tra} and the mixing layer height was low, suggesting that the contribution of vehicle emissions was affected more by the geographic distribution of emission sources and by wind direction than by the mixing layer height. In addition to the influences of meteorological conditions, low R_{tra} values occurred in polluted areas, and high R_{tra} values were accompanied by a low pollution concentration level during some periods (Fig. 10). The absolute concentration of pollutants from vehicle emissions was higher on polluted days because the dispersion was weak. However, relative contributions of vehicle emissions decreased, e.g., low R_{tra} values, on the polluted days because long-range transport also increased.

4. Conclusion

Vehicle emissions, such as nitrogen oxides, carbon monoxide, particulate matter, and volatile organic compounds, have become critical air pollutants in metropolitan areas. However, the temporal and spatial scales of urban-scale vehicle emissions vary widely. Differences in inter- and intra- vehicle emissions remain uncertain due to differences in vehicle types, vehicle speeds, driving cycles, roadway conditions, and other parameters in conventional vehicle emission inventories. In this study, vehicle emissions characteristics in the Greater Taipei Area were obtained using a vision-based traffic analysis system. The web-based traffic data were normalized, and the normalized diurnal cycle of vehicle emissions was applied to the CMAQ model to study the impacts of vehicle emissions on urban air quality.

The most common vehicles in Greater Taipei Area were sedans, followed by motorcycles. Vehicle compositions and traffic flow differed between weekdays and weekends. Moderate traffic conditions with an average speed of 30–50 km/h resulted in the highest average traffic flows during weekdays, whereas traffic flow was maximized when the average speed was 50–70 km/h during weekends. Traffic in free-flow

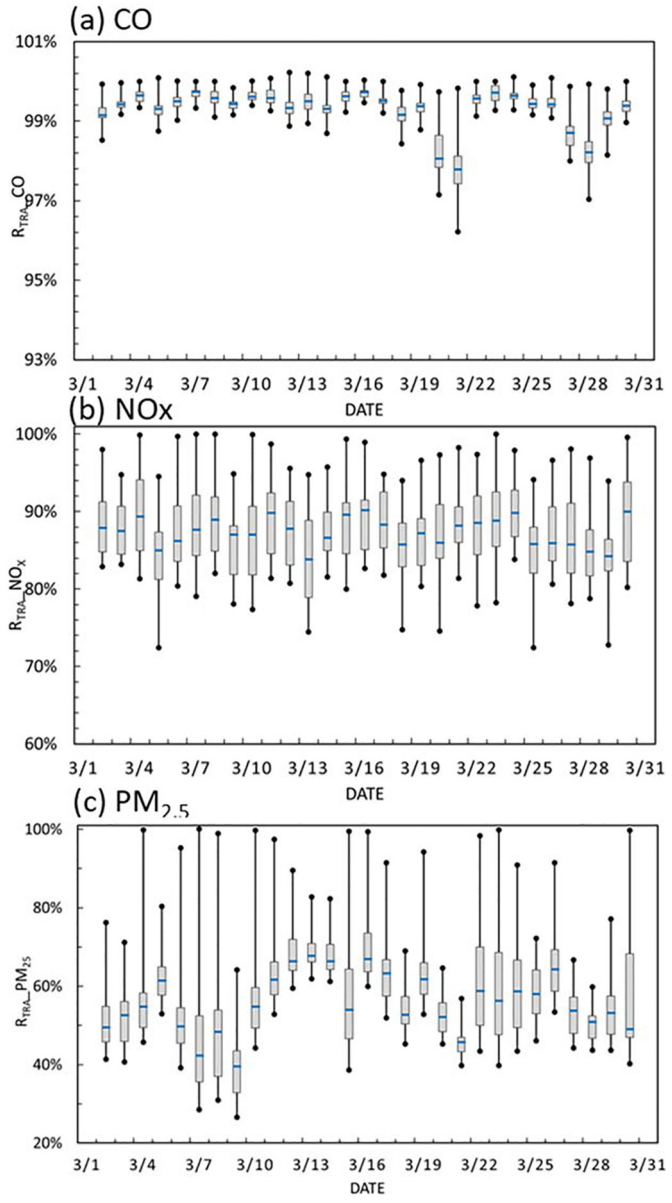

Fig. 9. Time series of daily vehicle emissions contributions, Rtra (%), to (a) CO, (b) NOx, and (c) $PM_{2.5}$ at EPA stations in the Taipei metropolitan area. Ranges are between the maximum and minimum *Rtra*, and the upper and lower limits of the box represent the interquartile range. The blue line is the mean value. (For interpretation of the references to color in this figure legend, the reader is referred to the web version of this article.)

conditions (>70 km/h) was more common on weekends than on weekdays. During weekends, the percentages of sedans in stopped-flow and free-flow traffic were lower than those on weekdays.

The differences between the diurnal cycles during weekdays and weekends revealed changes in human activity during weekends. Two peak traffic periods were identified during weekdays in the Greater Taipei Area: in the morning between 7:00 and 9:00 a.m. and in the afternoon starting at approximately 5:00 p.m. On weekends, the morning peak disappeared, and the variation in vehicle numbers was lower than that on weekdays.

The normalized diurnal cycles of vehicle emissions were applied to the regional air quality model. The simulation results suggested that the real-time traffic data improve the CMAQ model's performance, especially for CO and $PM_{2.5}$ concentrations. According to sensitivity tests with total emissions and vehicle emissions in the Greater Taipei Area, vehicle emissions contributed >90% to CO, 80% to NO_x, and

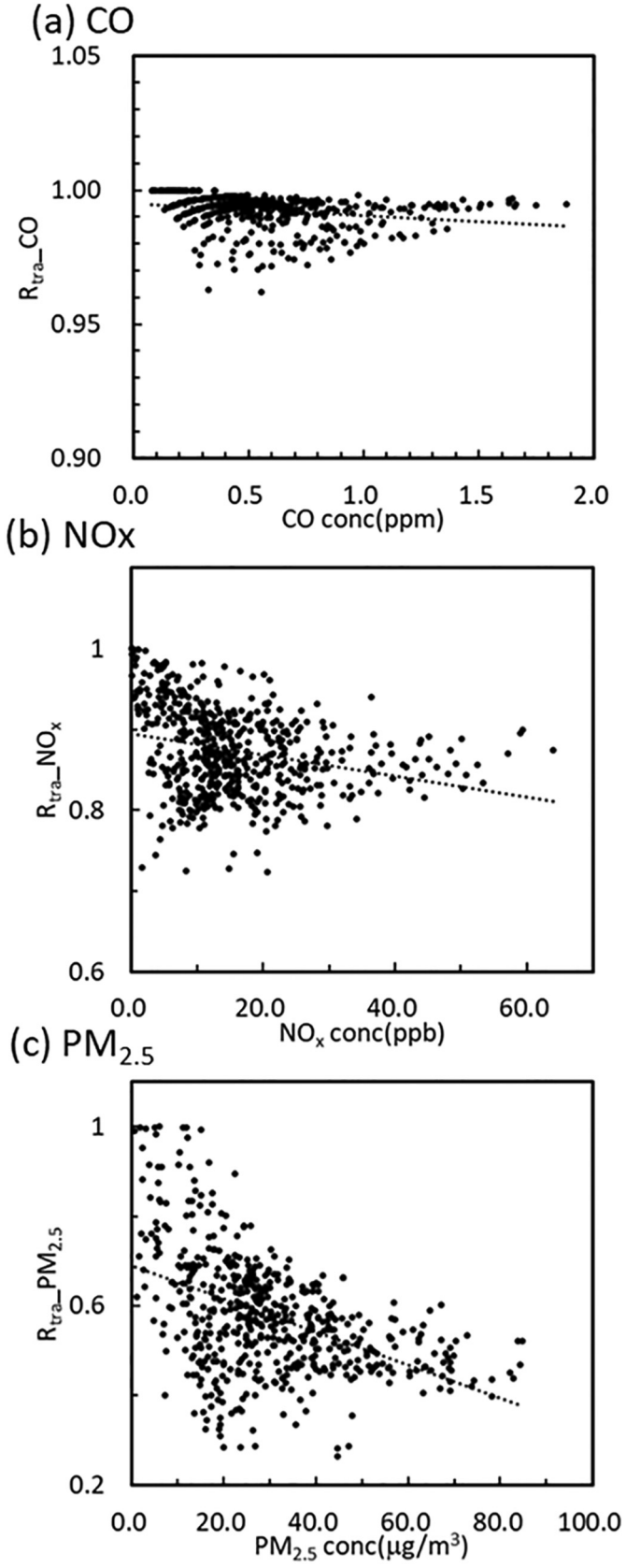

Fig. 10. Relationship between daily vehicle emissions contributions (*Rtra*) and mean concentrations of (a) CO (ppm), (b) NOx (ppb), and (c) $PM_{2.5}$ ($\mu g/m^3$) obtained from EPA stations in the Taipei metropolitan area during March 2019.

approximately 50% to $PM_{2.5}$ in downtown Taipei. The contribution of vehicle emissions was affected by vehicle emissions and meteorological conditions.

The variation in vehicle emissions in urban areas was significant, and the high spatiotemporal resolution of real-time traffic data enabled the presentation of local human and vehicle activities. The connection between surveillance camera data, vehicle emissions, and regional air quality models demonstrated in this study could also be used to explore the impacts of special events (e.g., long weekends and COVID-19 lockdowns) on air quality.

CRediT authorship contribution statement

I-Chun Tsai: Conceptualization, Investigation, Methodology, Software, Project administration, Supervision, Formal analysis, Visualization, Writing – original draft, Funding acquisition. **Chen-Ying Lee:** Data curation, Visualization. **Shih-Chun Candice Lung:** Funding acquisition, Writing – review & editing. **Chih-Wen Su:** Software, Writing – review & editing.

Declaration of competing interest

The authors declare that they have no known competing financial interests or personal relationships that could have appeared to influence the work reported in this paper.

Acknowledgment

We would like to acknowledge the funding support from Academia Sinica, Taiwan, under "Trans-disciplinary $PM_{2.5}$ Exposure Research in Urban Areas for Health-oriented Preventive Strategies ". Project No.: AS-SS-107-03 and AS-SS-110-02.

References

Alexey/AB, 2020. Darknet Yolo-v4 and Yolo-v3/v2 for Windows and Linux. Available online. https://github.com/AlexeyAB/darknet.

Anenberg, Susan C., Miller, Joshua, Minjares, Ray, Li, Du, Henze, Daven K., Lacey, Forrest, Malley, Christopher S., Emberson, Lisa, Franco, Vicente, Klimont, Zbigniew, Heyes, Chris, 2017. Impacts and mitigation of excess diesel-related NOx emissions in 11 major vehicle markets. Nature 545, 467–471.

Byun, Daewon, Schere, Kenneth L., 2006. Review of the governing equations, computational algorithms, and other components of the Models-3 community multiscale air quality (CMAQ) modeling system. Appl. Mech. Rev. 59, 51.

California Air Resources Board, 2018. EMFAC Web Database. Retrieved from California Air Resources Board:. https://www.arb.ca.gov/emfac/.

Carter, William P.L., 2000. 'Implementation of the SAPRC-99 chemical mechanism into the Models-3 framework. Report to the United States Environmental Protection Agency (January, 29).

Cui, J., Nelson, J.D., 2019. Underground transport: an overview. Tunn. Undergr. Space Technol. 87, 122–126. https://doi.org/10.1016/j.tust.2019.01.003.

Davis, N., Lents, J., Osses, M., Nikkila, N., Barth, M., 2005. Development and application of an international vehicle emissions model. Transp. Res. Rec. 1939 (1), 156–165. https://doi.org/10.1177/0361198105193900118.

Deng, C., Jin, Zhang, M., Liu, X., Yu, Z., 2018. Emission characteristics of VOCs from on-road vehicles in an urban tunnel in eastern China and predictions for 2017–2026. Aerosol Air Qual. Res. 18, 3025–3034. https://doi.org/10.4209/aaqr.2018.07.0248.

EPA, U, 2010. Motor Vehicle Emission Simulator (MOVES) User Guide. US Environmental Protection Agency.

European Environment Agency (EEA), 2019. Air quality in Europe—2019 report.

Filonchyk, M., Hurynovich, V., Yan, H., Gusev, A., Shpilevskaya, N., 2020. Impact assessment of COVID-19 on variations of SO2, NO2, CO and AOD over East China. Aerosol Air Qual. Res. 20, 1530–1540. https://doi.org/10.4209/aaqr.2020.05.0226.

Fu, Tzung-May, Jacob, Daniel J., Wittrock, Folkard, Burrows, John P., Vrekoussis, Mihalis, Henze, Daven K., 2008. Global budgets of atmospheric glyoxal and methylglyoxal, and implications for formation of secondary organic aerosols. J. Geophys. Res.-Atmos. 113.

Guenther, A., Karl, T., Harley, P., Wiedinmyer, C., Palmer, P.I., Geron, C., 2006. Estimates of global terrestrial isoprene emissions using MEGAN (Model of Emissions of Gases and Aerosols from Nature). Atmos. Chem. Phys. 6, 3181.

He, J., Wu, L., Mao, H., Liu, H., Jing, B., Yu, Y., Ren, P., Feng, C., Liu, X., 2016. Development of a vehicle emission inventory with high temporal–spatial resolution based on NRT traffic data and its impact on air pollution in Beijing – part 2: impact of vehicle emission on urban air quality. Atmos. Chem. Phys. 16, 3171–3184.

Hersbach, Hans, Dee, D.J.E.N., 2016. ERA5 reanalysis is in production. ECMWF newsletter 147, 5–6.

Hong, Song-You, Noh, Yign, Dudhia, Jimy, 2006. A new vertical diffusion package with explicit treatment of entrainment processes. Mon. Weather Rev. 134, 2318–2341.

Iacono, Michael J., Delamere, Jennifer S., Mlawer, Eli J., Shephard, Mark W., Clough, Shepard A., Collins, William D., 2008. Radiative forcing by long-lived greenhouse gases: Calculations with the AER radiative transfer models. J. Geophys. Res. 113 (D13103). https://doi.org/10.1029/2008JD009944.

Jing, Boyu, Wu, Lin, Mao, Hongjun, Gong, Sunning, He, Jianjun, Zou, Chao, Song, Guohua, Li, Xiaoyu, Zhong, Wu., 2016. Development of a vehicle emission inventory with high temporal–spatial resolution based on NRT traffic data and its impact on air pollution in Beijing–part 1: development and evaluation of vehicle emission inventory. Atmos. Chem. Phys. 16, 3161–3170.

Li, Nan, Tzung-May, Fu, Cao, Junji, Lee, Shuncheng, Huang, Xiao-Feng, He, Ling-Yan, Ho, Kin-Fai, Fu, Joshua S., Lam, Yun-Fat, 2013. Sources of secondary organic aerosols in the Pearl River Delta region in fall: contributions from the aqueous reactive uptake of dicarbonyls. Atmos. Environ. 76, 200–207.

Li, M., Zhang, Q., Kurokawa, J.I., Woo, J.H., He, K., Lu, Z., Ohara, T., Song, Y., Streets, D.G., Carmichael, G.R., Cheng, Y., Hong, C., Huo, H., Jiang, X., Kang, S., Liu, F., Su, H., Zheng, B., 2017. MIX: a mosaic Asian anthropogenic emission inventory under the international collaboration framework of the MICS-Asia and HTAP. Atmos. Chem. Phys. 17, 935–963.

Li, Xian, Lopes, D., Mok, K.M., Miranda, A.I., Yuen, K.V., Hoi, K.I., 2019. Development of a road traffic emission inventory with high spatial–temporal resolution in the world's most densely populated region—Macau. Environ. Monit. Assess. 191, 239.

Liu, Yong-Hong, Liao, Wen-Yuan, Li, Li, Huang, Yu-Ting, Wei-Jia, Xu., 2017. Vehicle emission trends in China's Guangdong Province from 1994 to 2014. Sci. Total Environ. 586, 512–521.

Marinello, S., Lolli, F., Gamberini, R., 2020. Roadway tunnels: a critical review of air pollutant concentrations and vehicular emissions. Transp. Res. Part D: Transp. Environ. 86. https://doi.org/10.1016/j.trd.2020.102478 (102478).

Marinello, S., Lolli, F., Gamberini, R., 2021. The impact of the COVID-19 emergency on local vehicular traffic and its consequences for the environment: the case of the City of Reggio Emilia (Italy). Sustainability 13 (1), 118.

Meng, Xiangrui, Zhang, Kaishan, Pang, Kaili, Xiang, Xinpeng, 2020. Characterization of spatio-temporal distribution of vehicle emissions using web-based real-time traffic data. Sci. Total Environ. 709, 136227.

Nagpure, A.S., Sharma, K., Gurjar, B.R., 2013. Traffic induced emission estimates and trends (2000–2005) in megacity Delhi. Urban Clim. 4, 61–73.

Ning, Z., Chan, T.L., 2007. On-road remote sensing of liquefied petroleum gas (LPG) vehicle emissions measurement and emission factors estimation. Atmos. Environ. 41 (39), 9099–9110. https://doi.org/10.1016/j.atmosenv.2007.08.006.

Redmon, J., Farhadi, A., 2018. YOLOv3: An Incremental Improvement. arXiv 2018 (arXiv: 1804.02767).

Silva, L.C.A., Dedini, F.G., Corrêa, F.C., Eckert, J.J., Becker, M., 2016. Measurement of wheelchair contact force with a low cost bench test. Med. Eng. Phys. 38 (2), 163–170. https://doi.org/10.1016/j.medengphy.2015.11.014.

Skamarock, W. C., J. B. Klemp, J. Dudhia, D. O. Gill, D. M. Barker, M. Duda, X.-Y. Huang, W. Wang and J. G. Powers. 2008. 'A Description of the Advanced Research WRF Version 3′, NCAR Technical Note.

Sun, Daniel(Jian), Ding, Xueqing, 2019. Spatiotemporal evolution of ridesourcing markets under the new restriction policy: A case study in Shanghai. Transp. Res. A Policy Pract. 130, 227–239. https://doi.org/10.1016/j.tra.2019.09.052.

Tao, W.-K., Simpson, Josh, Baker, D., Braun, S., Chou, M.-D., Ferrier, Brad, Johnson, D., Khain, Alexander, Lang, S., Lynn, Barry, Shie, Chung-Lin, Starr, David, Sui, Chung-Hsiung, Wang, Yi, Wetzel, P., 2003. Microphysics, radiation and surface processes in the Goddard Cumulus Ensemble (GCE) model. Meteorog. Atmos. Phys. 82, 97–137. https://doi.org/10.1007/s00703-001-0594-7.

Tewari, M., Chen, F., Wang, W., Dudhia, J., LeMone, M.A., Mitchell, K., Ek, M., Gayno, G., Wegiel, J., Cuenca, R.H., 2004. Implementation and verification of the unified NOAH land surface model in the WRF model. Paper Presented at the 20th Conference on Weather Analysis and Forecasting/16th Conference on Numerical Weather Prediction, Seattle, WA.

Tsai, I-Chun, Chen, Jen-Ping, Lung, Candice Shi-Chun, Li, Nan, Chen, Wei-Nai, Tzung-May, Fu, Chang, Chih-Chung, Hwang, Gong-Do, 2015. Sources and formation pathways of organic aerosol in a subtropical metropolis during summer. Atmos. Environ. 117, 51–60.

Wang, W.V., Lin, T.H., Liu, C.H., Su, C.W., Lung, S.C., 2020a. Fusion of environmental sensing on $PM_{2.5}$ and deep learning on vehicle detecting for acquiring roadside $PM_{2.5}$ concentration increments. Sensors (Basel, Switzerland) 20 (17), 4679. https://doi.org/10.3390/s20174679.

Wang, X., Wang, S., Cao, J., Wang, Y., 2020b. Data-driven based tiny-YOLOv3 method for front vehicle detection inducing SPP-net. IEEE Access 8, 110227–110236.

Wang, Z., Uno, I., Yumimoto, K., Itahashi, S., Chen, X., Yang, W., Wang, Z., 2021. Impacts of COVID-19 lockdown, spring festival and meteorology on the NO_2 variations in early 2020 over China based on in-situ observations, satellite retrievals and model simulations. Atmos. Environ. 244, 117972.

Wiedinmyer, C., Akagi, S.K., Yokelson, R.J., Emmons, L.K., Al-Saadi, J.A., Orlando, J.J., Soja, A.J., 2011. The fire INventory from NCAR (FINN): a high resolution global model to estimate the emissions from open burning. Geosci. Model Dev. 4, 625–641.

Zhang, Y., Wang, X., Li, G., Yang, W., Huang, Z., Zhang, Z., Huang, X., Deng, W., Liu, T., Huang, Z., Zhang, Z., 2015. Emission factors of fine particles, carbonaceous aerosols and traces gases from road vehicles: recent tests in an urban tunnel in the Pearl River Delta, China. Atmos. Environ. 122, 876–884.